

Cite this article as: Zhu Wenguang, Zhang Xin, Song Kangkai, et al. Effect of Ultrasonic Shot Peening on Fatigue Crack Growth Behavior of Commercial-Purity Zr[J]. Rare Metal Materials and Engineering, 2023, 52(08): 2711-2720.

ARTICLE

Effect of Ultrasonic Shot Peening on Fatigue Crack Growth Behavior of Commercial-Purity Zr

Zhu Wenguang¹, Zhang Xin^{1,2}, Song Kangkai¹, Wang Sui³, Zeng Xiangkang¹, Ma Chi¹, Zhang Conghui¹

¹ School of Metallurgical Engineering, Xi'an University of Architecture and Technology, Xi'an 710055, China; ² Northwest Institute for Nonferrous Metal Research, Xi'an 710016, China; ³ State Key Laboratory for Performance and Structure Safety of Petroleum Tubular Goods and Equipment Materials, CNPC Tubular Goods Research Institute, Xi'an 710077, China

Abstract: Double-side ultrasonic shot peening (USSP) was performed on a commercial-purity Zr plate with 2 mm in thickness. The effects of USSP on microstructure evolution and fatigue crack growth (FCG) behavior were investigated. Microstructure evolution was characterized by optical microscopy, laser confocal microscope, electron back-scatter diffraction, transmission electron microscope, and X-ray diffractometer. FCG tests were carried out using compact tension samples, the fracture morphology and crack growth path were analyzed accordingly. The results show that a refined surface gradient structure with compressive residual stress of about 250 μm in depth is formed after USSP treatment. The USSPed samples exhibit higher strength and surface roughness than the as-received samples. Notably, the fatigue crack growth life of USSP-8 min and USSP-12 min samples is increased by 28.1% and 50.9% compared to that of the as-received samples. The USSP treatment helps to improve the resistance to fatigue crack propagation, which in turn reduces the fatigue crack growth rate to a certain extent. The enhancement of the FCG performance can be ascribed to the combined effects of the compressive residual stress and the conspicuous grain refinement. Compressive residual stress enhances the crack closure effect and decreases the effective stress ratio. Meanwhile, grain refinement increases the fraction of grain boundary and decreases the cyclic plastic zone size, which is beneficial for crack growth resistance.

Key words: ultrasonic shot peening (USSP); commercial-purity Zr; fatigue crack growth; grain refinement; residual stress

Commercial-purity Zr which displays prominent high corrosion resistance, favorable mechanical properties and machinability has been widely applied to chemical industry such as reactors, pressure vessels, and pipelines^[1-2]. Fatigue failure is one of the most critical failure forms of such engineering components, which is extremely dangerous because there is no obvious sign until transient fracture^[3-4]. Hence, the improvement of fatigue resistance for commercial-purity Zr is very significant to ensure reliable operation of such components. Many studies have shown that surface strengthening treatment can enhance the properties of metallic materials. Shot peening (SP) is one of the most effective methods to improve the fatigue strength^[5-6]. Both compressive residual stress (CRS) and surface gradient structure formed by

high-speed projectile lead to the improved fatigue performance of the material^[7-8]. In contrast to conventional SP, ultrasonic shot peening (USSP) generates a deeper CRS layer with lower energy consumption and pollution, shorter processing time and more flexible of process parameters^[9-10], which is acknowledged to be a promising surface treatment method for metallic materials.

Studies have shown that surface strengthening treatment can significantly improve the fatigue performance of zirconium alloys^[9]. Xin et al^[11] reported that Zircaloy-4 alloy via surface mechanical rolling treatment possesses a longer fatigue life than the as-received sample. The enhancement of fatigue life can be attributed to the combined effects of the gradient ultra-fine structure and the gradient CRS. Wang et

Received date: February 03, 2023

Foundation item: National Natural Science Foundation of China (51674187); International Science and Technology Cooperation Projects of Shaanxi Province (2021KW-27); The Key Industry Chain (Group)-Industrial Field in Shaanxi Province (2019ZDLGY05-03)

Corresponding author: Zhang Conghui, Ph. D., Professor, School of Metallurgical Engineering, Xi'an University of Architecture and Technology, Xi'an 710055, P. R. China, Tel: 0086-29-82202547, E-mail: zhangconghui@xauat.edu.cn

Copyright © 2023, Northwest Institute for Nonferrous Metal Research. Published by Science Press. All rights reserved.

al^[12] found that the fatigue strength of pure Zr via surface treatment is increased by 23%. Zhang et al^[13] studied the initiation and propagation of fatigue cracks in USSP-treated pure Zr through microscopy and found that the crack initiation and propagation life of the USSP-treated pure Zr samples are 3.1 and 1.48 times higher than those of the as-received samples, respectively. Zhang^[14] and Pavan et al^[15] indicated that the CRS induced by laser shock peening reduces the FCG rate. Wang et al^[16] reported that SP has a positive effect on decreasing the short crack growth rate of Ti6-Al4-V, but exhibits negative effects on the long crack growth rate. Similar negative effects have been reported in other studies, which were mainly linked to the residual tensile stress during SP. Tensile stress reduces the crack closure effect, reducing fatigue performance accordingly^[17-18].

In general, surface strengthening treatment can improve the fatigue strength of metallic materials, whereas the effect of SP on the fatigue long crack growth rate is still controversial. Moreover, only a few studies have been made to reveal the effect of USSP on fatigue crack growth. The physical mechanism of USSP on fatigue crack growth behavior of commercial-purity Zr has seldom been thoroughly studied. In this work, the surface integrity of commercial-purity Zr subjected to USSP different times was observed. The tensile and FCG properties of USSP-treated samples were investigated and the mechanism of USSP treatment on FCG resistance was discussed as well.

1 Experiment

Hot-rolled and annealed commercial-purity Zr with an average grain size of about 20 μm was used, which contained impurities of 0.08C, 0.25(Fe+Cr), 0.012H, 0.05N, and 0.13O (wt%). Fig. 1 shows a schematic illustration of the USSP instrument. During USSP processing, the target surface received a severe plastic deformation due to the high power ultrasonic impact. The sample was treated by USSP at a vibration frequency of 20 kHz by stainless steel balls with a diameter of 3 mm. The distance between the horn and the treated sample was 7.5 mm with the duration of 8 and 12 min, respectively.

The microstructures of cross-sections and the surface topographies of the samples were characterized by optical microscopy (OM) and electron back-scatter diffraction (EBSD). For OM and EBSD analysis, the samples were

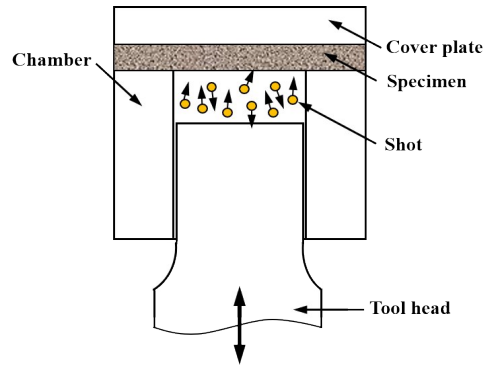


Fig.1 Schematic diagram of USSP process

mechanically polished with SiC abrasives to 3000#, then chemically etched in a reagent consisting of 2 mL HF, 9 mL HNO₃, and 9 mL C₃H₆O₃. A JEM-3010 high-resolution transmission electron microscope (TEM) was used to observe the surface microstructures of the USSP-treated samples. Sample preparation for TEM analysis includes pre-grinding to thicknesses of about 50 μm using SiC abrasives, followed by thinning with an electrolytic double-jet thinning instrument in the reagent of CH₂OH: HClO₄=1:19. Residual stresses were measured using X-ray diffraction (XRD) with Cu-K α radiation. Detailed experimental parameters for measuring the residual stress distribution of SP-treated samples can be found in our previous work^[19]. The fracture morphology and FCG path were observed by SEM which were cut from the compact tension samples. The local microstructural orientations of the crack tip were analyzed by EBSD.

FCG tests were performed on a 50 kN electro-hydraulic servo testing machine (Instron8801, USA) according to the GB/T 6398-2017 standard, China. Dimensions of the compact tensile (CT) sample employed were presented in Fig. 2a. Before the FCG rate test, 1.5 mm cracks were prefabricated according to the G-B/T 6398-2017 standard. The peening area is shown in Fig.2b on both sides of the sample. The loading direction is vertical to the rolling direction. The FCG tests were performed under constant load amplitude control for $R=0.1$ with a sinusoidal frequency of 10 Hz at room temperature. At least three samples were tested for each condition. The COD gauge was used to monitor the crack length. According to the measurement principle of the COD gauge given by the GB/T 6398-2017 standard, the flexibility U_x of a measurement

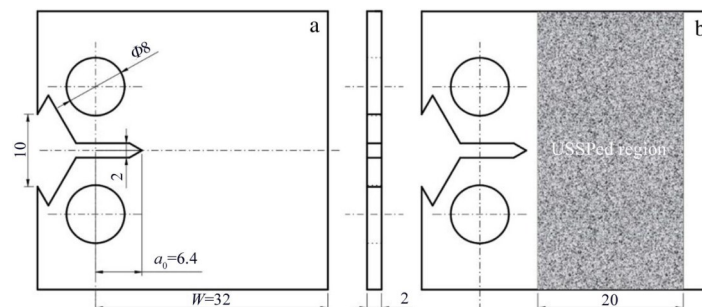


Fig.2 Schematic of the CT sample: (a) sample geometry and (b) USSP region on the CT sample

position was used as a function of the normalized crack length a/W , as shown in Eq.(1) and Eq.(2).

$$U_x = \left\{ \left[\frac{BEV_x}{F} \right]^2 + 1 \right\}^{-1} \quad (1)$$

$$\frac{a}{W} = C_0 + C_1 U_x + C_2 U_x^2 + C_3 U_x^3 + C_4 U_x^4 + C_5 U_x^5 \quad (2)$$

where E is the elastic modulus, U_x is the displacement of the measuring point. COD gauge is clamped at V_0 position, $C_0 = 1.0010$, $C_1 = -4.6695$, $C_2 = 18.460$, $C_3 = -236.82$, $C_4 = 1214.9$, $C_5 = -2143.6$.

The following equation was used to determine the stress intensity factor (SIF, ΔK)^[17]:

$$\Delta K = \frac{\Delta P}{B\sqrt{W}} \cdot \frac{(2+\alpha)}{(1-\alpha)^{3/2}} (0.886 + 4.64\alpha - 13.32\alpha^2 + 14.72\alpha^3 - 5.6\alpha^4) \quad (3)$$

where ΔP is the applied load range, B is the sample thickness, and α is the aspect ratio (crack length/sample width, $\alpha = a/W$). The crack length and the corresponding cycle number were recorded. The incremental polynomial method was used to fit the $a-N$ curve and to derive da/dN . In most cases, FCG rates are assumed to follow the Paris formula^[20]:

$$da/dN = C(\Delta K)^m \quad (4)$$

where da/dN is the fatigue crack growth rate, ΔK is the SIF range, C and m are the material parameters.

2 Results

2.1 Microstructure evolution during USSP

Fig. 3 shows the optical cross-section microstructure and surface morphologies of commercial-purity Zr before and after USSP treatment. As seen in Fig. 3a, the as-received sample exhibits an equiaxed microstructure with an average grain size of 20 μm . Noticeable grain refinement takes place owing to the high strain rate and gradient strain on the surface of the samples induced by USSP. With increasing processing time, the grain refinement effect and the thickness of the deformed layer increase significantly. After USSP for 8 and 12 min, the thickness of plastically deformed layer is 175 and 219 μm , respectively, as seen in Fig.3c and 3e. Fig.3b, 3d, and 3f exhibit the surface morphology and roughness value which increases from 1.07 μm to 4.55 μm after USSP treatment. The impact of the high-speed shots increases the roughness of the samples during USSP treatment. The slight decrease in surface roughness to 3.78 μm of USSP-12 min sample may be attributed to the work-hardening effect induced by previous multiple impacts^[21].

To further analyze the microstructure evolution before and after USSP, the cross-section of the samples was characterized by EBSD. Fig.4a–4c present the EBSD images of as-received sample. As seen from Fig.4a, the as-received sample consists of uniform equiaxed structure, and no twins can be observed. Fig. 4b shows the grain boundary and misorientation angle

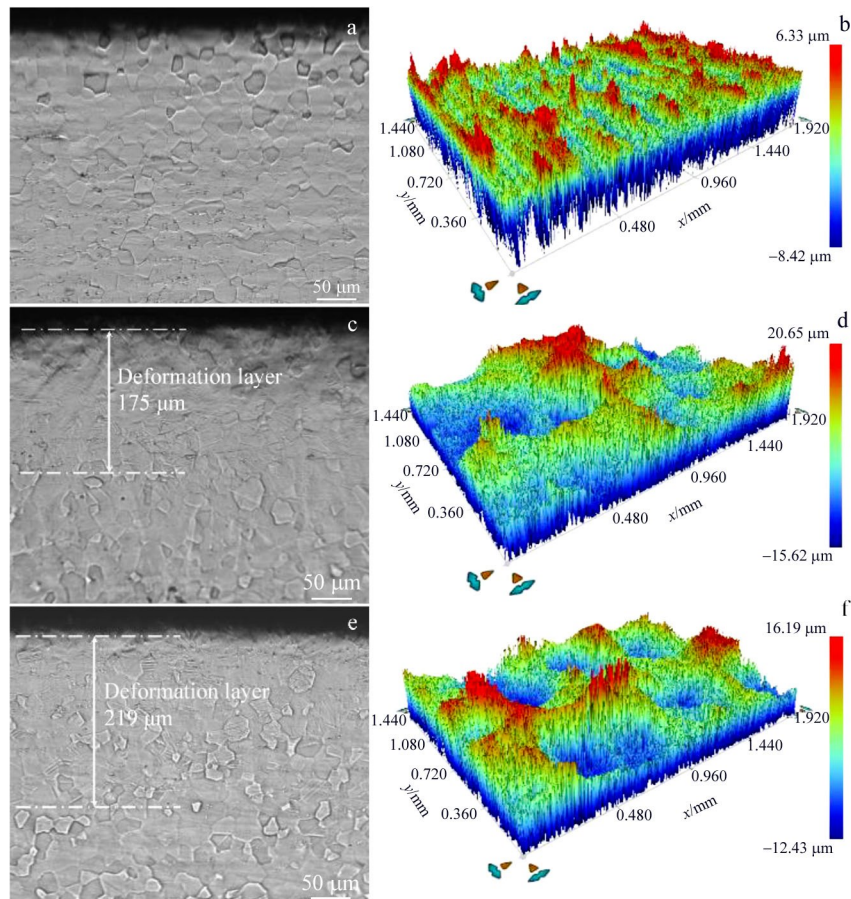


Fig.3 Cross-sectional and surface morphologies of different samples: (a–b) as-received, (c–d) USSP-8 min, and (e–f) USSP-12 min

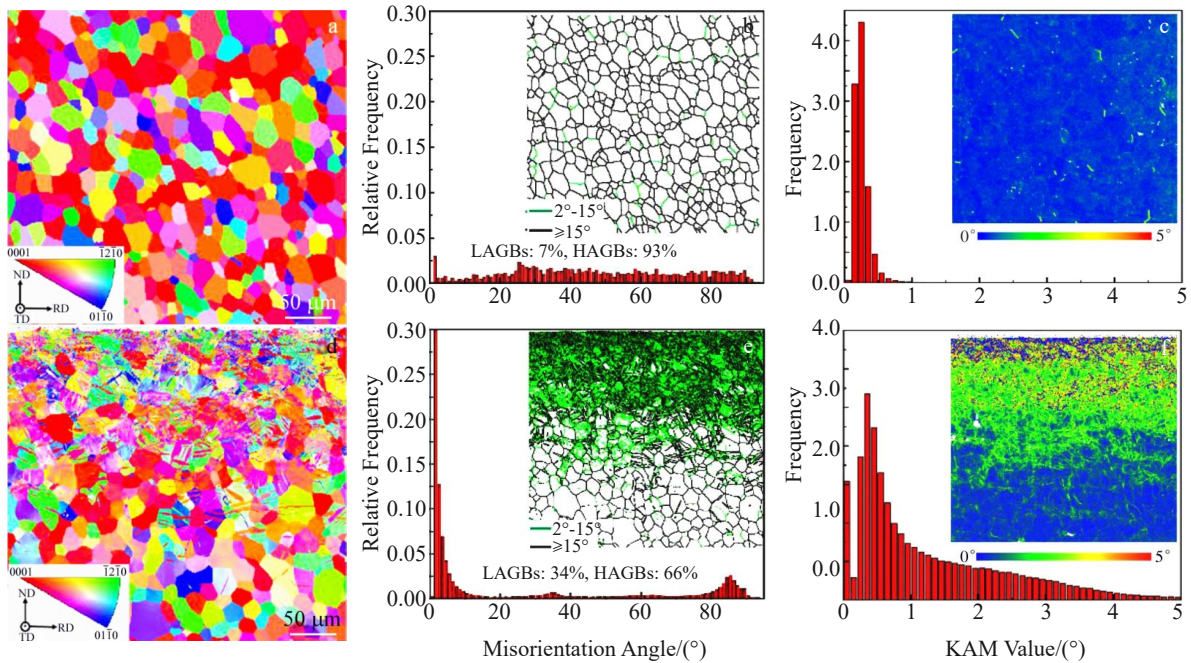


Fig.4 EBSD characterization of the microstructures of as-received sample (a–c) and USSP-12 min sample (d–f): (a, d) IPF map, (b, e) grain boundary and misorientation angle distributions, and (c, f) KAM distribution

distributions. The green lines and black lines represent low angle grain boundaries (LAGBs) and high angle grain boundaries (HAGBs), respectively. In the as-received sample, grain boundaries are mainly HAGBs, and the ratio of HAGB:LAGB is 7%:93%. Kernel average misorientation (KAM) maps are used to evaluate the degree of the local misorientations. Fig. 4c shows the KAM maps and the corresponding fraction of the as-received sample. The results show that the as-received sample has a low KAM value. Likewise, the EBSD images of the USSP-12 min sample are shown in Fig. 4d–4f. Fig. 4d shows a gradient microstructure with notably refined grain on the surface layer. The top refined region is barely resolved by EBSD due to extremely refined grain and the high residual strain. From the depth of 25 μm to the matrix, there is a large amount of deformation twinning. Commercial-purity Zr (α -Zr) possesses a hexagonal close-packed structure with limited number of slip systems. Thus, twinning becomes an important mode to accommodate deformation. Due to severe plastic deformation during USSP, a large number of dislocations and subgrain boundaries are generated, resulting in an increase in LAGBs in the surface layer (Fig. 4e). As shown in Fig. 4f, the KAM value of surface layer is significantly higher than that of the matrix region. However, the region near the top surface, which undergoes the highest plastic deformation, shows a lower KAM value than the subsurface layer region. Similar results are explained by the dynamic recrystallization in the near-surface region^[22].

Fig. 5 shows the TEM image and the corresponding selected area electron diffraction (SAED) pattern at surface area of the USSP-12 min sample. The bright-field image displays that the grains on the top surface of the USSP-12 min sample have been refined to nanograins with a grain size less than 100

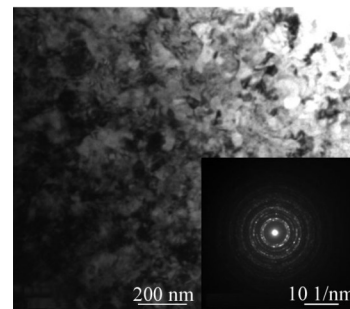


Fig.5 TEM image and SAED pattern of USSP-12 min sample

nm. This result is verified by SAED pattern as well, which consists of a series of continuous rings, indicating that these nano-sized grains possess random crystallographic orientations.

2.2 Effect of USSP on residual stress and tensile properties

Fig. 6 shows the residual stress distribution along the depth after USSP treatment. During USSP process, different local nonreversible plastic deformation between the surface layer and the interior is introduced, which causes strain gradient and leads to the residual stress^[23]. As seen in Fig. 6, the compressive residual stress (CRS) increases gradually to a maximum value and then decreases. This trend is owing to energy transformation during USSP treatment. The impact of the shot results in higher plastic constraint in the near-surface layer than in the deep surface layer. Thus, the maximum CRS is generated at the sub-surface. With the increase in USSP durations, both the maximum CRS and its depth are increased. The maximum CRS of USSP-8 min and USSP-12 min samples is about -354 and -394 MPa, and the corresponding depths are about 80 and 96 μm , respectively.

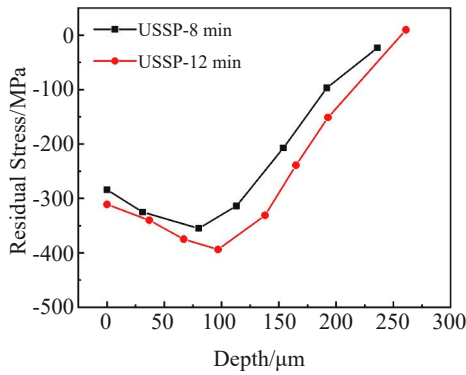


Fig.6 Residual stress distribution along different depths

Fig. 7 presents the tensile properties of the USSPed commercial-purity Zr. As seen from Fig. 7a, both the ultimate tensile strength (UTS) and yield strength (YS) increase apparently after USSP treatment, while the ductility decreases. The yield strength, tensile strength, and total elongation of the as-received samples are 275 MPa, 460 MPa, and 33.2%,

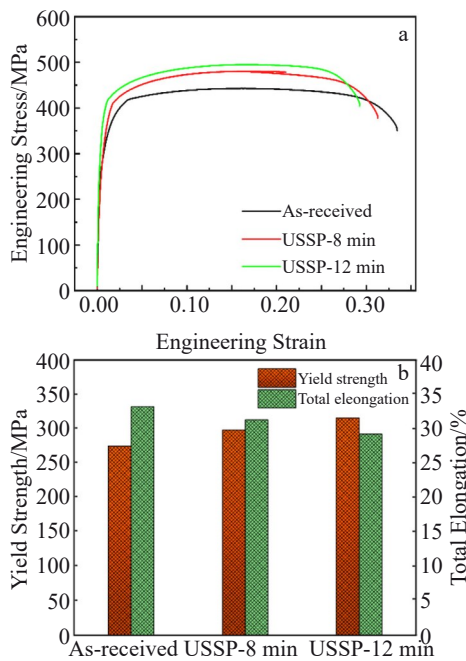


Fig.7 Engineering stress-strain curves (a) and tensile properties (b) of the as-received and USSPed samples

respectively. The YS increases to 298 and 316 MPa, and the UTS increases to 480 and 495 MPa, after USSP for 8 and 12 min, respectively; on the contrary, the total elongation decreases to 31.3% and 29.25%, respectively. This strength improvement is attributed to a combination of the following two factors: (1) formation of the gradient nanostructures layer on the sample surface, (2) CRS induced by USSP. However, the fall in ductility may be attributed to the increase in surface roughness and the work-hardening effect.

2.3 Effect of USSP on fatigue crack growth behavior

Fig. 8 shows the crack length as a function of the number of fatigue cycles for as-received and USSP samples. The prefabricated crack length a_0 is about 8 mm. As seen from Fig. 8, the FCG rate increases with the increase in cyclic number N , suggesting an approximately exponential growth. The crack in the as-received sample grow to 22.7 mm in length, and after 59 709 cycles, the sample is broken. For USSP-8 min and USSP-12 min samples, the corresponding crack length and fatigue life are 23.0 mm (76 492 cycles), and 23.2 mm (90 099 cycles), respectively. The FCG rate of the USSPed samples is significantly slower than that of the as-received samples. Compared with the as-received sample, the fatigue crack growth life is increased by 28.1% and 50.9% after USSP treatment for 8 and 12 min, respectively.

Fig. 9 shows the FCG rate (da/dN) for as-received and USSP samples. It can be seen that the FCG rate increases with the increment in ΔK . The FCG rate of the as-received sample is the fastest under the same ΔK . Generally, the whole fatigue

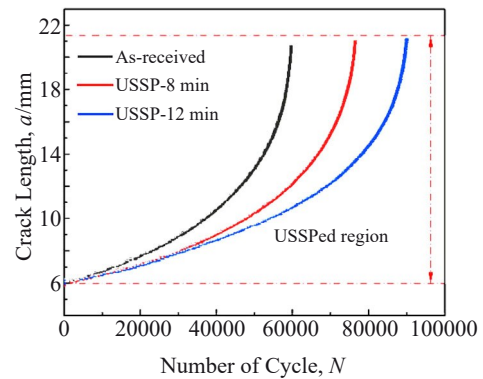


Fig.8 Crack length as a function of fatigue cycles in the as-received and USSP samples

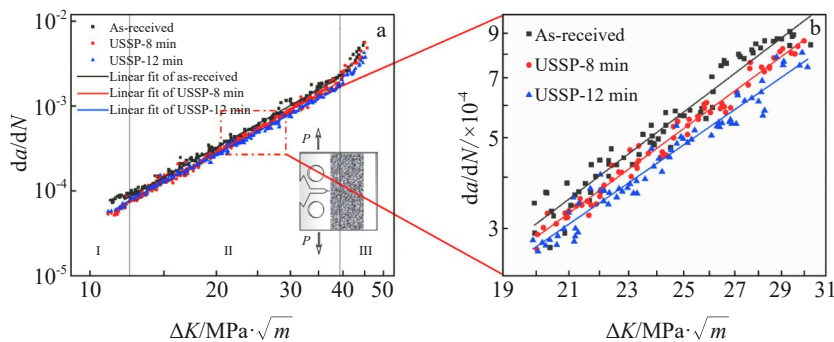


Fig.9 FCG rate of the as-received and USSPed samples: (a) da/dN - ΔK curve and (b) close-up of region II

crack growth process can be roughly divided into three regions according to the growth rate^[14]: the initial region with an unstable-growth rate (I), the stable-growth region (II), and the rapid-growth region (III). The relationship between ΔK and da/dN in region II can be regarded as a linear relationship in double logarithmic coordinates. The Paris formula was adopted to fit the relationship of the curves, and the calculated C and m constant values of Eq.(2) can be found in Table 1. After USSP treatment, the C value increases while the m value decreases. These changes indicate that the FCG rate of USSP samples decreases, especially when the peening duration is increased. As seen in Fig.9, a close-up view of the stable-growing stage is displayed and a slight difference in FCG rate is observed. Grain refinement and complex CRS induced by shot peening result in an improvement in FCG resistance^[14,24], so the FCG rate of USSP-8 min and USSP-12 min samples is lower than that of the as-received samples, especially for USSP-12 min samples. In the rapid expansion stage, the crack rapidly propagates at almost the same rate until fracture. As the residual area of the specimen decreases, the crack growth rate is gradually controlled by the fracture toughness of the material.

To further investigate the FCG behavior of commercial-purity Zr before and after USSP treatment, fatigue crack trajectory and fractured surface morphology in different regions of the as-received and USSP-12 min samples are observed. Fig. 10 shows micrographs of different locations along crack growth paths. At the crack length $a=10.5$ mm, the distance between the fatigue crack flanks in the as-received

sample is approximately 127.1 μm (Fig. 10a) and decreases with increasing the crack length, which is 65.3 μm when the crack length is 16.0 mm (Fig. 10b). In contrast, the USSP-12 min sample shows a significantly smaller distance between the fatigue crack flanks which is approximately 105.5 μm at the crack length $a=10.5$ mm (Fig. 10d), and decreases to approximately 53.9 μm when $a=16$ mm (Fig. 10e). According to the distance between the fatigue crack flanks, it is clear that the crack opening area of the USSP samples is smaller than that of the as-received sample, indicating that USSP is beneficial to retarding crack growth. In the as-received sample, the crack propagates in an approximately straight and smooth manner (Fig. 10c). However, the cracks in the USSP-12 min sample exhibit a tortuous pattern (Fig. 10f), which can also be observed in Fig.10d and 10e. The tortuous crack path can reduce the effective driving force for crack growth, thus improving the fatigue crack growth resistance^[25-26].

To further analyze the effect of USSP on FCG, the crack tip on the subsurface layer was characterized by EBSD. Fig. 11 shows the crystallographic orientation maps and corresponding KAM maps near the crack tip with the corresponding ΔK of 27 $\text{MPa}\cdot\text{m}^{1/2}$. Compared with the as-received sample, more crack bifurcations and deflections appear on the USSP-12 min sample, as shown in Fig. 11a and 11b. Crack bifurcation and deflection reduce the crack-driving force at the crack tip, resulting in fatigue crack growth deceleration^[27]. In addition, twinning activity occur around the crack, which is parallel to each other. Particularly, in the USSP-12 min sample, there are more deformation twins as seen in Fig. 11b. As shown in Fig. 11c and 11d, the degree of local misorientation near the crack tip is characterized by the KAM map. Under cyclic loading, obvious evidence of plastic deformation is seen along the cracks. Such deformation degree is relatively low in the as-received sample. Compared with the as-received sample, the sub-surface layer of USSP samples produces greater plastic deformation in the front of the cracks. The relatively high

Table 1 Material constants C and m for as-received and USSPed samples

Sample	C	m	R^2
As-received	4.79E-8	2.93	0.995
USSP-8 min	6.03E-8	2.83	0.993
USSP-12 min	9.33E-8	2.66	0.994

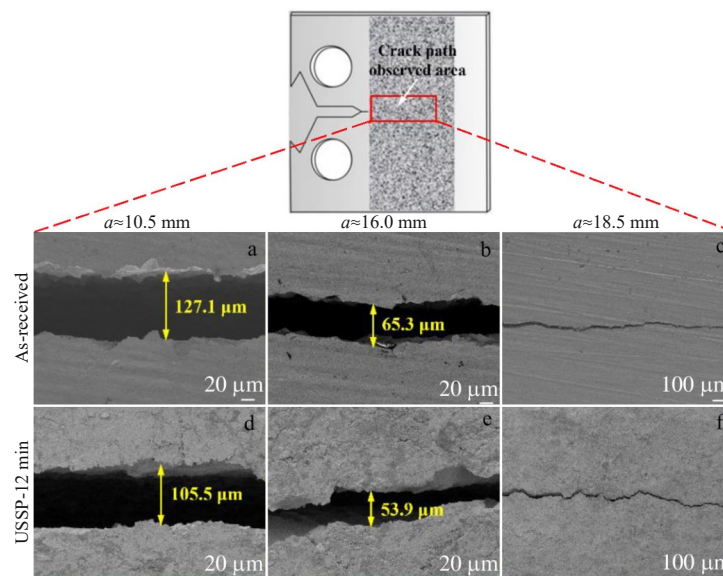


Fig.10 SEM micrographs of crack growth at different positions for as-received (a–c) and USSP-12 min (d–f) samples

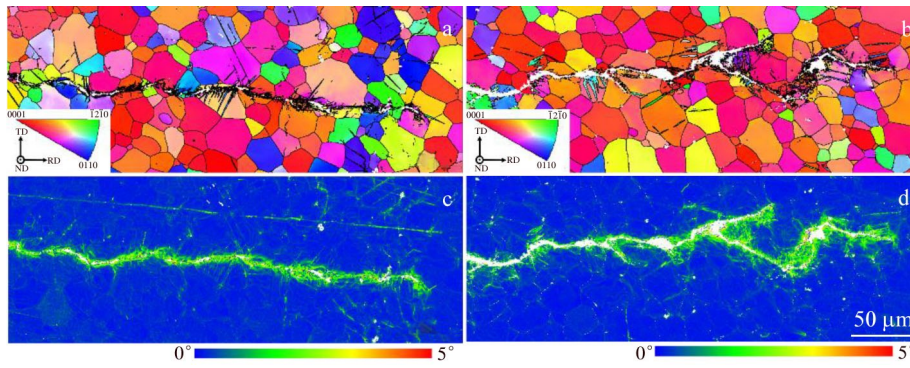


Fig.11 Crystallographic orientation maps and corresponding KAM maps at the crack tip for as-received (a, c) and USSP-12 min (b, d) samples

local deformation can reduce the stress concentration at the crack tip^[28]. Thus, the FCG driving force decreases, thereby enhancing the FCG resistance.

Fig.12 shows the fracture morphologies at different regions of commercial-purity Zr plate before and after USSP treatment. Typical features in region I of the as-received sample are tearing ridges, fatigue striations, and cleavage steps, as shown in Fig. 12a and 12b. The fracture morphology of the near-surface layer of the USSP sample (Fig. 12f) is different from that of other regions, showing a serrated fracture surface with small and intermittent tearing edges and many secondary cracks. The fracture features in the mid-thickness region of the USSP sample (Fig. 12k) display large secondary cracks, tearing ridges, and fatigue striations. Such

differences are associated with the distinct residual stress state and microstructure feature at the surface. The FCG path of the USSP sample is more circuitous, and the fracture morphology shows more secondary cracks^[29], which can decelerate the crack growth. The FCG rate of materials can be determined indirectly by fatigue striations spacing^[30]. Fig. 12b, 12g, and 12l show the enlarged view of region I. The fatigue striation spacing of the USSP sample is smaller than that of the as-received sample.

Fig. 12c, 12h, and 12m illustrate the morphologies of region II. Clear fatigue striation and secondary cracks can be seen in the as-received sample, as well as in the mid-thickness region of the USSP sample. However, the near-surface of the USSP sample (Fig. 12h) has no obvious fatigue striation and the

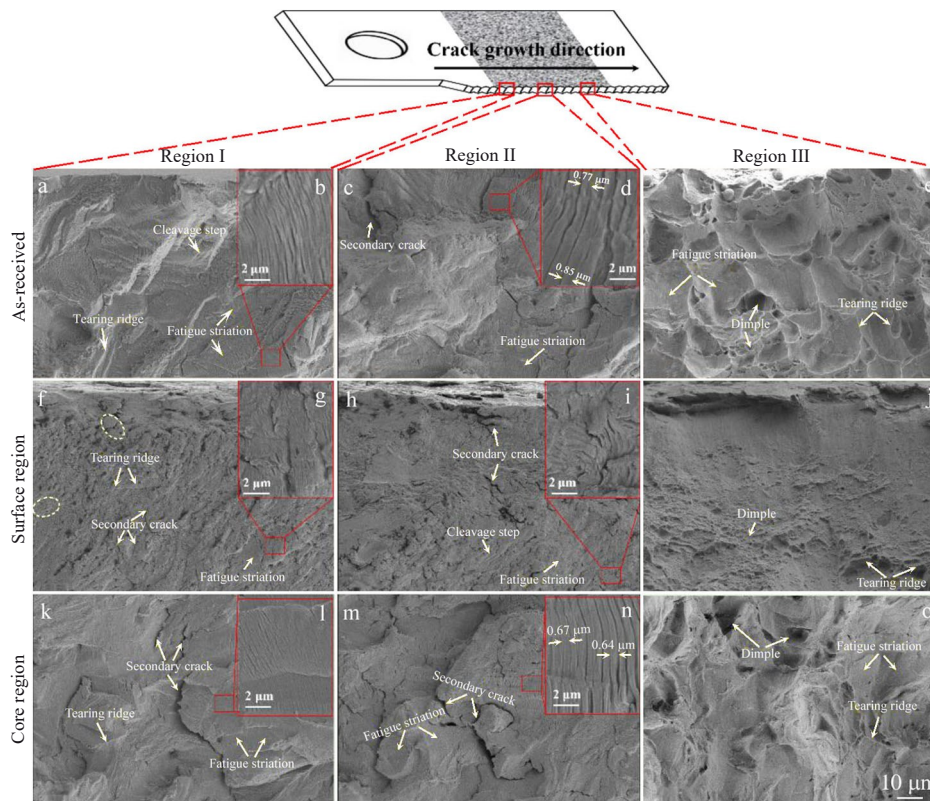


Fig.12 SEM morphologies of the fractured surface of different regions for as-received (a–e), near-surface area of USSP-12 min (f–j), and mid-thickness area of USSP-12 min (k–o)

fractured surface becomes relatively smooth. The smooth crack surface may be due to grain refinement and the friction between the crack surfaces caused by CRS during cyclic loading. Interestingly, a large number of secondary cracks are identified in the USSP sample, which plays a significant role in decelerating the FCG. Compared with region I, the fatigue striations spacing in region II is significantly increased. It can be seen from the enlarged view of region II (Fig. 12d, 12i, and 12n) that the crack growth rate of the USSP sample is still lower than that of the as-received sample.

The fracture morphologies in region III of as-received and USSP samples are shown in Fig. 12e, 12j, and 12o. There are dimples with different sizes and a large number of tearing edges on the fracture surface of samples. Due to the increase in local stress, the crack growth mode gradually changes from fatigue fracture to ductile fracture. It can be seen that the size of the dimples in the as-received sample is the largest, indicating that the elongation and the plastic deformation in the fractured region of the sample are the largest. Compared with untreated samples, the size of the dimple in the near-surface layer of USSP sample is the smallest due to grain refinement and CRS.

3 Discussion

3.1 Effects of grain refinement on the FCG

From the analysis of Fig. 4, it can be seen that USSP treatment generates significant grain refinement on the surface layer of commercial-purity Zr. This refinement provides more grain boundaries for impeding dislocation movement, hence improving the yield strength. Grain boundaries act as barriers for the crack growth. Massive grain boundaries produced by USSP lead to more energy consumption. Thus, the crack growth rate decreases.

Generally, the local stress and strain near the crack tip control the FCG process^[31]. The FCG rate is controlled by the maximum SIF K_{\max} and the SIF range ΔK . The maximum SIF K_{\max} controls the uniaxial plastic zone size, and the SIF range ΔK controls the cyclic plastic zone size. Under cyclic loading, the cyclic plastic deformation at the crack tip accumulates continuously, leading to crack growth. The size of the cyclic plastic zone at the crack tip can be written as^[32]:

$$r_c = \frac{1}{3\pi} \left(\frac{\Delta K}{2\sigma_y} \right)^2 \quad (\text{plane stress}) \quad (5)$$

where ΔK is the SIF range ($\text{MPa}\cdot\text{m}^{1/2}$), and σ_y is the yield strength of the materials (MPa).

Because the thickness of the CT specimen used in this FCG experiment is 2 mm, it belongs to a thin specimen and is under plane stress conditions. According to Eq.(5), we calculated the size of the cyclic plastic zone of as-received and USSP-12 min samples, as shown in Fig. 13. The USSP-12 min sample has a smaller size of the cyclic plastic zone than the as-received sample at the same ΔK . The size of the cyclic plastic zone is the main driving force for FCG under cyclic loading^[33-34]. From Eq.(5), it can be easily understood that the increase in σ_y will lead to the decrease in cyclic plastic zone r_c . This result

means that USSP treatment can reduce r_c . Thus, the driving force of crack growth and the rate of crack growth is reduced.

According to Irwin's research^[35], the ΔK describes the stress state at a crack tip, which can also be expressed as Eq.(6):

$$\Delta K = Y\Delta\sigma\sqrt{\pi a} \quad (6)$$

where Y is the coefficient of the fatigue crack shape, σ is the stress of the load, and a is the crack length.

In polar coordinates (r, θ), the plastic deformation zone at the crack tip r_y can be expressed as Eq.(7) and the ΔK can be expressed as Eq.(8)^[36]:

$$r_y = \frac{1}{4\pi\sqrt{2}} \left(\frac{\Delta K}{\sigma_y} \right)^2 \quad (7)$$

$$\Delta K = Y\Delta\sigma\sqrt{\pi(a+r_y)} \quad (8)$$

Substituting Eq.(7) into Eq.(8), ΔK can be expressed as:

$$\Delta K = \frac{Y\Delta\sigma\sqrt{\pi a}}{\sqrt{1 - \frac{Y^2}{4\sqrt{2}} \left(\frac{\Delta\sigma}{\sigma_y} \right)^2}} \quad (9)$$

From Eq.(9), σ_y will affect the modified SIF range ΔK . It can be seen that the increase in σ_y will lead to the decrease in the modified SIF range ΔK , and the decrease in ΔK will lead to the decrease in fatigue crack growth rate. According to Fig. 7, USSP treatment increases the yield strength of commercial-purity Zr. This is because of the effect of grain refinement after shot peening, which provides more grain boundaries to prevent dislocation movement and increases the difficulty of dislocations passing through grain boundaries, thereby increasing the yield strength^[37]. Thus, constrained dislocation motion and higher yield strength contribute to the decrease in ΔK and smaller plastic zone, delaying fatigue crack propagation^[38]. Hence, according to the value of the SIF range, the crack growth driving force for the USSP-12 min sample is the lowest, resulting in the lowest crack growth rate. Therefore, USSP treatment improves FCG resistance of commercial-purity Zr.

3.2 Effects of compressive residual stress on FCG

USSP treatment induces a CRS field about 200–300 μm to the surface of commercial-purity Zr, which has an important impact on the FCG performance. According to the

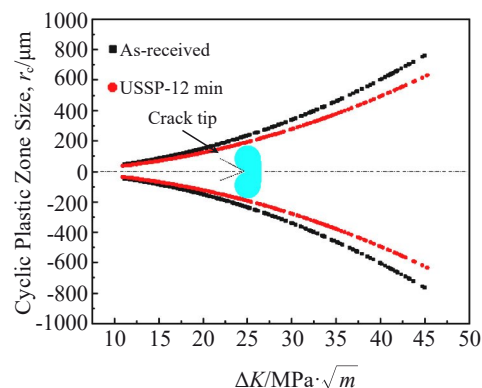


Fig.13 Cyclic plastic zone size at the crack tip for as-received and USSP-12 min samples

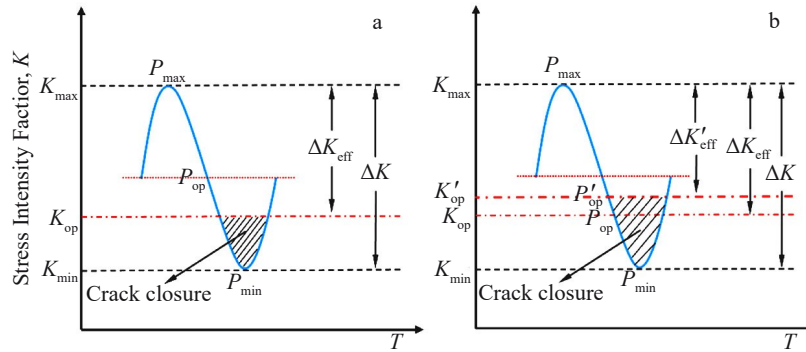


Fig.14 Schematic of crack closure without (a) and with (b) USSP

superposition principle^[39], the CRS introduced by USSP can be linearly superimposed on the stresses generated by the applied mechanical loads. The total stress intensity factor at the crack tip is the sum of the SIF (K_{crs}) associated with the CRS and the SIF (K_{app}) caused by the applied load during the cyclic loading^[39]:

$$K_{max,tot} = K_{max,app} + K_{crs} \quad (10)$$

$$K_{min,tot} = K_{min,app} + K_{crs} \quad (11)$$

where $K_{max,app}$ and $K_{min,app}$ are the SIFs at the maximum and minimum applied loads during the cyclic loading, respectively. The total stress ratio is calculated as follows:

$$\Delta K_{tot} = K_{max,app} - K_{min,app} \quad (12)$$

$$R_{tot} = \frac{K_{min,tot}}{K_{max,tot}} = \frac{K_{min,app} + K_{crs}}{K_{max,app} + K_{crs}} \quad (13)$$

From Eq.(12) and Eq.(13), it can be seen that the SIF range is not affected by the CRS, while the total stress ratio depends on the CRS. With the increase in stress ratio, the fatigue crack growth rate gradually increases^[40]. The CRS induced by USSP reduces the total stress ratio and the crack growth rate.

Crack closure is an inherent phenomenon in crack growth. The introduced surface residual compressive stress is the internal stress distributed in all directions, so there is a direction parallel to the applied load. For mode I crack, the applied load is perpendicular to the crack surface, which is in the same direction as the residual compressive stress generated by shot peening. Due to the linear superposition of applied load and residual compressive stress, the effective stress decreases^[42]. As seen in Fig.14a, Elber^[41] argued that there is a critical crack opening loads P_{op} , and the fatigue crack can expand when the applied loads are higher than this value. Considering the crack closure effect, Elber proposed the concept of the effective driving force and considered that K_{op} reduces the SIF range from ΔK to ΔK_{eff} according to Eq. (14):

$$\Delta K_{eff} = K_{max,app} - K_{op} \quad (14)$$

where K_{op} is the SIF caused by the crack opening loads, and ΔK_{eff} is the effective SIF range.

As seen in Fig.14b, the CRS induced by USSP increases the value of crack opening loads from P_{op} to P'_{op} , resulting in the early contact of two crack surfaces and the increase in crack closure interval. After USSP treatment, the effective SIF range at the crack tip can be given by Eq. (15):

$$\Delta K'_{eff} = K_{max,app} - K_{op} + K_{crs} \quad (15)$$

According to Eq. (14) and Eq. (15), it can be known that crack closure includes the inherent closure of the material and the additional closure caused by CRS. The CRS introduced by USSP reduces the effective SIF range, resulting in a decrease in the effective crack growth driving force. Thus, the FCG rate of USSPed samples decreases, especially the USSP-12 min sample.

4 Conclusions

1) A surface gradient structure with high compressive residual stress forms. The depth of gradient structure layer and compressive residual stress field increases with increasing USSP time.

2) The yield strength of the USSP-12 min sample is 15% higher than that of the as-received sample, which is attributed to the synergy effects of grain refinement, dislocation strengthening, and compressive residual stress.

3) USSP treatment can reduce the fatigue crack growth rate to a certain extent. After USSP treatment for 8 and 12 min, the fatigue crack growth life is increased by about 28.1% and 50.9%, respectively. The enhancement of fatigue crack growth resistance is originated from both the enhanced crack closure effect and stress ratio reduction caused by compressive residual stress and the decrease in cyclic plastic zone size caused by surface grain refinement.

References

- 1 Yang J N, Zhang L J, Ning J et al. *International Journal of Refractory Metals & Hard Materials*[J], 2018, 73: 58
- 2 Hu X, Zhao H, Song N et al. *Materials Characterization*[J], 2017, 129: 149
- 3 Yang C, Xu W, Guo B et al. *Materials*[J], 2016, 9(8): 641
- 4 Zhao X H, Wang M Y, Zhang Z Q et al. *Materials*[J], 2016, 9(6): 471
- 5 Qin Z, Li B, Zhang H et al. *Engineering Failure Analysis*[J], 2022, 133: 106 010
- 6 Nie L, Wu Y, H Gong et al. *Materials*[J], 2020, 13(14): 3169
- 7 Shi H, D Liu, Y Pan et al. *International Journal of Fatigue*[J], 2021, 151: 106 391

- 8 Qi Y, Zhou W, Zhong Y et al. *International Journal of Fatigue*[J], 2017, 107: 83
- 9 Chen H, Guan Y J, Zhu L H et al. *Materials Chemistry and Physics*[J], 2021, 259: 124 025
- 10 Moon J H, Baek S M, Lee S G et al. *Materials Research Letters*[J], 2019, 7(3): 97
- 11 Xin C, Sun Q Y, Xiao L et al. *Journal of Materials Science*[J], 2018, 53: 12 492
- 12 Wang Yaomian, Cheng Jiapeng, Zhang Conghui. *Rare Metal Materials and Engineering*[J], 2019, 48(8): 2574 (in Chinese)
- 13 Zhang C H, Song G D, Wang Y M et al. *Materials Science and Engineering A*[J], 2020, 794: 139 831
- 14 Zhang H P, Cai Z Y, Chi J X et al. *Journal of Alloys and Compounds*[J], 2021(6): 161 427
- 15 Pavan M, Furfari D, Ahmad B et al. *International Journal of Fatigue*[J], 2019, 123: 157
- 16 Wang Y, Zhang Y, Song G et al. *Materials Today Communications*[J], 2020, 25: 101 430
- 17 Bergant Z, Trdan U, Grum J. *International Journal of Fatigue*[J], 2016, 87: 444
- 18 Chahardehi A, Brennan F P, Steuwer A. *Engineering Fracture Mechanics*[J], 2010, 77(11): 2033
- 19 Xiao G Z, Zhang X, Zhang C H et al. *Coatings*[J], 2022, 12(2): 131
- 20 Paris P. *J Basic Eng*[J], 1963, 85(4): 528
- 21 Zhang Q, Duan B B, Zhang Z Q et al. *Journal of Materials Research and Technology*[J], 2021, 11: 1090
- 22 Li X, Sun B H, Guan B et al. *International Journal of Fatigue*[J], 2021, 146: 106 142
- 23 Chen M, Jiang C H, Xu Z et al. *Surface and Coatings Technology*[J], 2019, 359: 511
- 24 Nikolai K, Volker V, Manfred H et al. *International Journal of Fatigue*[J], 2017, 98 : 223
- 25 Pippan R, Hohenwarter A. *Fatigue & Fracture of Engineering Materials & Structures*[J], 2017, 40(4): 471
- 26 Zhang H J, Zhao X H, Liu Y. *International Journal of Fatigue*[J], 2021, 147: 106 172
- 27 Suresh S. *Metallurgical Transactions A*[J], 1983, 14(11): 2375
- 28 Feng J C, Li L Q, Chen Y B et al. *Optics & Laser Technology*[J], 2021, 134: 106 668
- 29 Yuan C W, Li S C, Huang J et al. *Materials Characterization*[J], 2021, 174: 111 041
- 30 Sheng J, Huang S, Zhou J Z et al. *Optics and Laser Technology*[J], 2016, 77: 169
- 31 Noroozi A H, Glinka G, Lambert S. *International Journal of Fatigue*[J], 2005, 27(10) : 1277
- 32 Rice J R. *Journal of Applied Mechanics*[J], 1967, 34(2): 287
- 33 Peng J, Gao Y, Dai Q et al. *Acta Metallurgica Sinica*[J], 2019, 55(6): 773
- 34 Kim J H, Lee S B. *Theoretical & Applied Fracture Mechanics*[J], 2000, 34(1): 73
- 35 Irwin G R. *Applied Fracture Mechanics*[J], 1957, 24: 361
- 36 Shih C F, Asaro R J. *Applied Fracture Mechanics*[J], 1988, 55 (2): 299
- 37 Xin C, Sun Q Y, Xiao L et al. *Journal of Materials Engineering and Performance*[J], 2019, 28(10): 6354
- 38 Sun R J, Li L H, Guo W et al. *Materials Science & Engineering A*[J], 2018, 737: 94
- 39 LaRue J E, Daniewicz S R. *International Journal of Fatigue*[J], 2006, 29(3): 508
- 40 Bilir Ömer G, Harun Metin. *Engineering Fracture Mechanics*[J], 1990, 37(6) : 1203
- 41 Elber W. *ASTM STP*[J], 1971, 486: 230

超声喷丸对工业纯 Zr 疲劳裂纹扩展行为的影响

朱文光¹, 张鑫^{1,2}, 宋慷慨¹, 王遂³, 曾祥康¹, 马驰¹, 张聪惠¹

(1. 西安建筑科技大学 冶金工程学院, 陕西 西安 710055)

(2. 西北有色金属研究院, 陕西 西安 710016)

(3. 中国石油天然气集团公司管材研究所 石油管材及设备材料性能与结构安全国家重点实验室, 陕西 西安 710077)

摘要: 对厚度为2.0 mm的工业纯锆板材进行双面超声喷丸(USSP)处理, 研究了超声喷丸(USSP)对微观组织演变和疲劳裂纹扩展(FCG)行为的影响。通过光学显微镜、激光共聚焦显微镜、背散射电子衍射仪、透射电子显微镜和X射线衍射仪分别对微观结构演变进行表征。采用紧凑拉伸试样进行FCG试验, 对断口形貌和裂纹扩展路径进行分析。结果表明, USSP处理后形成了具有约250 μm深度残余压应力的表面梯度结构, USSP试样比原始试样表现出更高的强度和表面粗糙度。值得注意的是, USSP-8 min和USSP-12 min试样的疲劳裂纹扩展寿命比原始试样分别提高了28.1%和50.9%。USSP处理有助于提高疲劳裂纹扩展抗力, 进而在一定程度上降低疲劳裂纹的扩展速率。FCG性能的提高可归因于残余压应力和晶粒细化的共同作用, 残余压应力增强了裂纹闭合效应, 降低了有效应力比。同时, 晶粒细化使晶界比例增加, 循环塑性区尺寸减小, 从而有利于抵抗裂纹扩展。

关键词: 超声喷丸(USSP); 工业纯Zr; 疲劳裂纹扩展; 晶粒细化; 残余应力

作者简介: 朱文光, 男, 1987年生, 博士, 西安建筑科技大学冶金工程学院, 陕西 西安 710055, E-mail: szhuwg@xauat.edu.cn